NJC

PAPER

View Article Online
View Journal | View Issue

Cite this: *New J. Chem.*, 2025, **49**, 17743

Thiol–ene click functionalization of a MCM-41/Fe_3O_4 nanocomposite with acrylic acid: a magnetically recoverable solid acid catalyst for efficient conversion of sugars to 5-HMF

Abdul R Mkia,[a] Suhas Ballal,[b] Shaker Al-Hasnaawei,[cd] Shelesh Krishna Saraswat,[e] Subhashree Ray,*[f] Naveen Chandra Talniya,[gh] Aashna Sinha[i] and Vatsal Jain[j]

Received 20th July 2025,
Accepted 10th September 2025

DOI: 10.1039/d5nj02955d

rsc.li/njc

The development of efficient solid acid catalysts is critical for the sustainable production of 5-hydroxymethylfurfural (5-HMF), an important foundational chemical obtained from biomass. In this work, mesoporous silica MCM-41 was prepared and modified with Fe_3O_4 nanoparticles to impart magnetic recoverability. The surface was further functionalized with 3-mercaptopropyltriethoxysilane to introduce thiol groups, followed by a thiol–ene click reaction with acrylic acid to graft carboxylic acid functionalities onto the surface. The resulting magnetically recoverable nanocomposite was comprehensively characterized using FT-IR spectroscopy, acid–base titration, EDX, XRD, BET, TEM, SEM, TGA, and VSM analyses. The nanocomposite combined the high surface area and ordered mesoporosity of MCM-41 with the magnetic separability of Fe_3O_4 nanoparticles. It was used as a solid acid catalyst for the transformation of sugars into 5-HMF. The influences of several reaction parameters like the reaction temperature, catalyst amount, reaction time, and type of solvent were assessed for the transformation of fructose into 5-HMF. The optimized reaction conditions were determined to be a temperature of 120 °C, 30 mg of catalyst, a reaction time of 1 h, and the reaction medium with a dimethyl sulfoxide/H_2O (V/V) ratio of 2/1. Under these conditions, the conversion of fructose resulted in 94% 5-HMF yield. The catalyst also demonstrated outstanding reusability across multiple cycles with a minimal loss of effectiveness. Moreover, the turnover number (TON) and turnover frequency (TOF) were calculated to be 25.2 and 25.2 h^{-1}, respectively, highlighting the efficiency of our developed catalytic system.

1. Introduction

Today, the world's attention to green technologies and pollution reduction is increasing.[1–4] The growing environmental issues linked to the use of fossil fuels and the rising demand for sustainable energy and chemicals have driven significant research into biomass conversion technologies.[5–8] Among numerous platform chemicals obtained from biomass, 5-hydroxymethylfurfural (5-HMF) has attracted considerable attention owing to its versatile applications as a pivotal intermediate for biofuels, bioplastics, and pharmaceuticals.[9,10] 5-HMF contains both aldehyde and hydroxymethyl functional groups, as well as a furan ring, making it highly versatile for downstream chemical transformations.[11] 5-HMF can be synthesized through the acid-catalyzed dehydration of hexose sugars like fructose and glucose, and its efficient production is critical for the development of a sustainable biorefinery.[12,13]

The conversion of sugars into 5-HMF typically requires acidic conditions, and although homogeneous acid catalysts such as HCl and H_2SO_4 have shown high catalytic activity, they

[a] *Faculty of Allied Medical Sciences, Hourani Center for Applied Scientific Research, Al-Ahliyya Amman University, Amman, Jordan*
[b] *Department of Chemistry and Biochemistry, School of Sciences, JAIN (Deemed to be University), Bangalore, Karnataka, India*
[c] *College of Pharmacy, The Islamic University, Najaf, Iraq*
[d] *Department of Medical Analysis, Medical Laboratory Technique College, The Islamic University of Al Diwaniyah, Al Diwaniyah, Iraq*
[e] *Department of ECE, GLA University, Mathura-281406, India*
[f] *Department of Biochemistry, IMS and SUM Hospital, Siksha 'O' Anusandhan (Deemed to be University), Bhubaneswar, Odisha-751003, India. E-mail: subhashreeray@soa.ac.in*
[g] *Department of Chemistry, Graphic Era Hill University, Dehradun, India*
[h] *Centre for Promotion of Research, Graphic Era Deemed to be University, Dehradun, Uttarakhand-248002, India*
[i] *School of Applied and Life Sciences, Division of Research and Innovation, Uttaranchal University, Dehradun, Uttarakhand, India*
[j] *Centre for Research Impact & Outcome, Chitkara University Institute of Engineering and Technology, Chitkara University, Rajpura, 140401, Punjab, India*

pose several drawbacks including corrosion, difficulty in separation, and environmental hazards.[14] To overcome these issues, heterogeneous acid catalysts (solid acids) have gained attention as promising alternatives.[15–17] These include sulfonated carbon materials, metal oxides, heteropoly acids supported on porous supports, zeolites, and functionalized mesoporous silica. Solid acid catalysts offer significant advantages such as ease of separation, recyclability, tunable acidity, and reduced environmental impact.[18,19] Moreover, the use of bifunctional catalysts combining Brønsted and Lewis acid sites has been found to enhance the conversion of more recalcitrant sugars like glucose and disaccharides by promoting isomerization-dehydration tandem reactions.[20,21] In this context, surface functionalization of various solid support materials with acidic groups has been widely employed to develop solid acid catalysts for the transformation of sugars into 5-HMF.[22,23]

Among numerous solid supports, mesoporous silica MCM-41 has gained prominence due to its unique structural and textural properties, including a highly ordered hexagonal arrangement of uniform mesopores, large surface area, and tunable pore sizes.[24–26] Moreover, the high thermal and mechanical stability of MCM-41 makes it a suitable support for a wide range of catalytic reactions under different operating conditions.[27] In addition, the surface of MCM-41 can be easily functionalized or modified to anchor various metal ions, nanoparticles, or organometallic complexes, enabling the design of tailored catalytic systems.[28]

Despite the high effectiveness of MCM-41-based catalytic systems, their practical application is often hindered by difficulties in separation from the reaction mixture. Owing to their fine powder form and lack of magnetic properties, conventional MCM-41 catalysts require time-consuming and energy-intensive separation techniques such as filtration or centrifugation, which can result in catalyst loss and reduced process efficiency.[29] Therefore, enhancing the separability of MCM-41 materials is essential to fully exploit their catalytic potential in practical applications. This issue can be effectively addressed by incorporating magnetic Fe_3O_4 nanoparticles into the MCM-41 framework. The magnetic properties of Fe_3O_4 facilitate easy separation and recycling of the catalyst using an external magnet, enhancing the overall efficiency and sustainability of catalytic processes.[30–34] The incorporation of Fe_3O_4 can improve the separation of the MCM-41 framework, while maintaining its high surface area and uniform pore structure.[35–39]

On the other hand, the covalent attachment of catalytically active sites to solid supports represents a pivotal strategy in the design and development of heterogeneous catalysts. In this regard, the thiol–ene click reaction has emerged as a particularly attractive method owing to its regioselectivity, high efficiency, mild reaction conditions, and broad functional group compatibility.[40,41] This radical-mediated addition of thiols to alkenes proceeds rapidly under ambient conditions and often requires only photochemical or thermal initiation, making it highly suitable for surface functionalization without compromising the structural integrity of the support or the catalytic moiety.[42] Consequently, the thiol–ene click reaction offers a robust and versatile platform for the immobilization of catalytic active species on a variety of solid supports, thereby advancing the design of efficient and recoverable heterogeneous catalytic systems.

Herein, we reported the synthesis of a novel magnetically recoverable heterogeneous acid catalyst based on MCM-41 functionalized with Fe_3O_4 nanoparticles, followed by surface modification with 3-mercaptoprpopyltriethoxysilane through the post-synthesis method and subsequent thiol–ene click functionalization with acrylic acid. Using this strategy, acrylic acid, a carboxylic acid-containing molecule, can be covalently attached to the modified surface, thereby introducing Brønsted acid sites that are essential for the conversion of sugars to 5-HMF. The catalyst was thoroughly characterized using different physicochemical techniques and evaluated for its catalytic performance in the synthesis of 5-HMF from sugars including fructose, glucose, sucrose, maltose, and cellulose. The influences of reaction parameters and catalyst reusability were also systematically examined in the dehydration of fructose to 5-HMF.

2. Experimental

2.1. General

All chemicals utilized in this work were obtained from Sigma-Aldrich and utilized without further purification. All solvents were of analytical grade and used as supplied. Deionized water was used throughout the experiments. The prepared materials were thoroughly characterized *via* a range of analytical methods such as Fourier-transform infrared spectroscopy (FT-IR), energy-dispersive X-ray spectroscopy (EDX), X-ray diffraction (XRD), Brunauer–Emmett–Teller (BET) analysis, transmission electron microscopy (TEM), scanning electron microscopy (SEM), vibrating sample magnetometry (VSM), acid–base titration, thermogravimetric analysis (TGA), and nuclear magnetic resonance (NMR) spectroscopy. Detailed information on the instrumentation and characterization procedures is given in the SI.

2.2. Synthesis of mesoporous silica MCM-41

Mesoporous silica MCM-41 was prepared based on the experimental procedure reported in the literature.[43] In a typical procedure, 2.5 g of cetyltrimethylammonium bromide (CTAB) was dissolved in 50.0 mL of deionized water under constant stirring. After complete dissolution, 60.0 g of ethanol and 16.8 g of ammonium hydroxide (25%) were added to modify the pH to around 11. Subsequently, 4.7 g of tetraethyl orthosilicate (TEOS) was added dropwise to the solution under vigorous stirring. The mixture was stirred at room temperature for 2 h. The obtained white solid was isolated by filtration, rinsed several times with deionized water and ethanol, and dried at 80 °C overnight. The dried solid was calcined at 550 °C for 6 h to remove the surfactant template, affording pure mesoporous silica MCM-41.

2.3. Synthesis of the magnetic MCM-41 nanocomposite (MCM-41/Fe_3O_4)

The magnetic MCM-41 nanocomposite (MCM-41/Fe_3O_4) was prepared *via* an *in situ* co-precipitation method. Briefly, 1.0 g

of MCM-41 was dispersed in 100.0 mL of deionized water using ultrasonication for 30 min. Then, $FeCl_2{\cdot}4H_2O$ (4.0 mmol, 0.8 g) and $FeCl_3{\cdot}6H_2O$ (8.0 mmol, 1.1 g) were added to the dispersion under a nitrogen atmosphere. The mixture was heated to 80 °C under mechanical stirring. Subsequently, 20.0 mL of ammonium hydroxide (25%) was added dropwise to initiate the precipitation of Fe_3O_4. The reaction mixture was maintained at 80 °C for 2 h. The resulting black solid was magnetically separated, rinsed several times with deionized water and ethanol, and then dried at 80 °C overnight.

2.4. Synthesis of mercaptopropyl-functionalized MCM-41/Fe_3O_4 (MCM-41/Fe_3O_4-SH)

Typically, 1.0 g of MCM-41/Fe_3O_4 was dispersed in 50.0 mL of anhydrous toluene under a nitrogen atmosphere. Then, 1.0 mL of 3-mercaptoprpopyltriethoxysilane (MPTES) was added, and the mixture was refluxed for 24 h under continuous stirring. After cooling to room temperature, mercaptopropyl-functionalized MCM-41/Fe_3O_4 (MCM-41/Fe_3O_4-SH) was isolated using a magnet, rinsed thoroughly with toluene and ethanol to remove unreacted MPTMS, and dried at 80 °C overnight.

2.5. Synthesis of acrylic acid-functionalized MCM-41/Fe_3O_4 (MCM-41/Fe_3O_4–COOH)

The MCM-41/Fe_3O_4-SH was further modified with acrylic acid through a thiol–ene click reaction. In a typical procedure, 1.0 g of MCM-41/Fe_3O_4-SH was dispersed in 50.0 mL of chloroform under a nitrogen atmosphere. To this, 2.0 mmol of acrylic acid and benzoyl peroxide (0.1 mmol) were added as initiators. The mixture was refluxed for 2 h under continuous stirring. After completion, the obtained product (MCM-41/Fe_3O_4–COOH) was separated using an external magnet, rinsed thoroughly with chloroform to remove unreacted reagents, and then dried at 80 °C overnight.

2.6. General method for the catalytic dehydration of fructose to 5-HMF over MCM-41/Fe_3O_4–COOH

In a typical experiment, fructose (100.0 mg) and the desired amount of MCM-41/Fe_3O_4–COOH were added to a sealed reactor containing 3.0 mL of solvent. The reaction mixture was stirred and heated at the desired temperature (ranging from 80 to 140 °C) for a specified duration (15–60 min). Upon completion, the reaction mixture was allowed to cool to room temperature, and the catalyst was magnetically removed from the reaction mixture. The liquid phase was diluted with ethyl acetate as the extracting solvent to extract 5-HMF and then subjected to solvent removal under reduced pressure. The 5-HMF was purified by column chromatography on a silica gel utilizing an appropriate eluent (*e.g.*, ethyl acetate/hexane). The purified 5-HMF was analyzed by NMR and FT-IR spectroscopy and the yield of 5-HMF was calculated based on the initial amount of fructose used, as follows:

$$\text{5-HMF yield (\%)} = [\text{moles of 5-HMF formed/moles of preliminary fructose}] \times 100\%$$

3. Results and discussion

The catalyst was prepared following the methodology presented in Scheme 1. The synthetic procedure began with the preparation of mesoporous silica MCM-41, providing a high surface area and a uniform pore structure ideal for further functionalization. Subsequently, MCM-41 was modified by incorporating

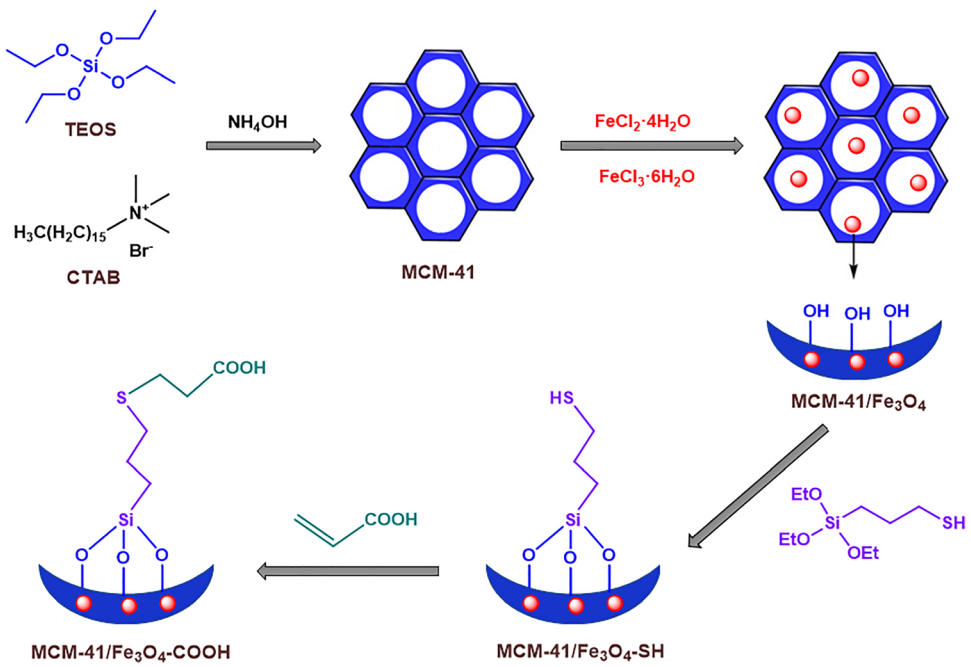

Scheme 1 Synthesis procedure of MCM-41/Fe_3O_4–COOH.

Fe_3O_4 nanoparticles, producing the MCM-41/Fe_3O_4 nanocomposite with magnetic properties for easy separation. The surface of MCM-41/Fe_3O_4 was then functionalized with MPTES to introduce thiol groups, yielding mercaptopropylated MCM-41/Fe_3O_4 (MCM-41/Fe_3O_4-SH). Finally, a thiol–ene click reaction was carried out between the surface thiol groups and acrylic acid, leading to the covalent attachment of carboxylic acid groups onto the surface of MCM-41/Fe_3O_4 (MCM-41/Fe_3O_4–COOH).

FT-IR spectroscopy was used to confirm the effective surface functionalization of MCM-41, as shown in Fig. 1. The spectra of all samples exhibited characteristic bands at 1085 cm^{-1} and 800 cm^{-1}, corresponding to the asymmetric and symmetric stretching vibrations of Si–O–Si, along with a band at 460 cm^{-1} attributed to the bending vibration of Si–O–Si, confirming the mesoporous silica framework.[44,45] Upon incorporation of Fe_3O_4 nanoparticles, a band appeared at 593 cm^{-1} in the spectrum of MCM-41/Fe_3O_4 due to the Fe–O stretching vibration, approving the successful preparation of the MCM-41/Fe_3O_4 nanocomposite.[46,47] Functionalization with MPTES introduced some bands at about 2800–3000 cm^{-1} in the spectrum of MCM-41/Fe_3O_4-SH, corresponding to the –CH stretching vibration in methylene groups from the MPTES, verifying the successful grafting of thiol groups.[48] Further modification *via* the thiol–ene click reaction with acrylic acid resulted in the emergence of a new band around 1735 cm^{-1} in the spectrum of MCM-41/Fe_3O_4–COOH, characteristic of C=O stretching from carboxylic acid groups.[13,49] These spectral changes collectively confirmed the stepwise surface modification of the MCM-41/Fe_3O_4 nanocomposite.

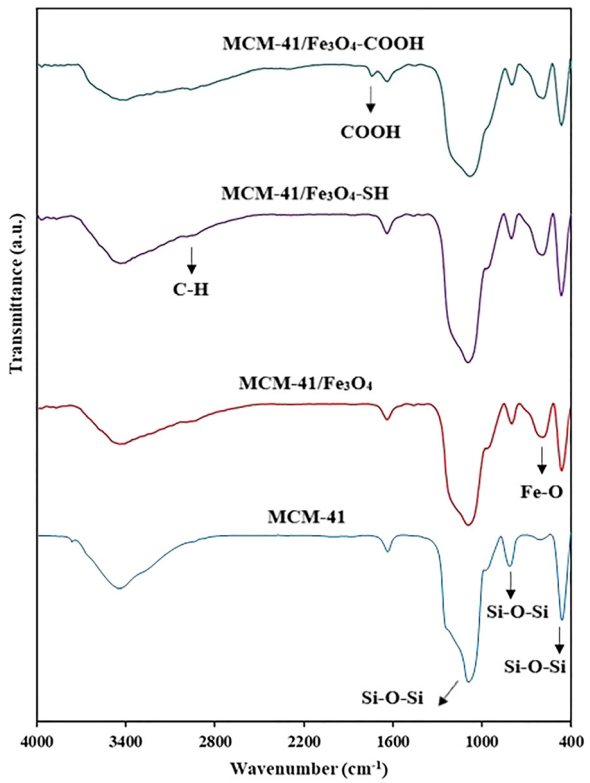

Fig. 1 FT-IR spectra of MCM-41, MCM-41/Fe_3O_4, MCM-41/Fe_3O_4-SH, and MCM-41/Fe_3O_4–COOH.

EDX spectroscopy was employed to analyze the elemental composition of MCM-41/Fe_3O_4–COOH. The EDX spectrum of MCM-41/Fe_3O_4–COOH (Fig. 2a) revealed the presence of key elements including silicon (Si), oxygen (O), iron (Fe), sulfur (S), and carbon (C). The EDX mapping images (Fig. 2b–f) further showed a uniform distribution of Si, O, Fe, S, and C across the catalyst, suggesting homogeneous surface modification.

The acid–base titration experiment was performed to calculate the amount of carboxylic acid groups introduced *via* the thiol–ene click reaction with acrylic acid. According to the titration result, the quantity of carboxylic acid groups in MCM-41/Fe_3O_4–COOH was 0.69 mmol g^{-1}.

XRD analysis was conducted to explore the crystal structures of MCM-41, MCM-41/Fe_3O_4, and MCM-41/Fe_3O_4–COOH (Fig. 3). The XRD pattern of pure MCM-41 revealed a wide peak at about 20–30° corresponding to amorphous silica.[50] After incorporation of Fe_3O_4 nanoparticles, characteristic diffraction peaks at 2θ = 30.3°, 35.6°, 43.4°, 53.8°, 57.3°, and 62.8° were observed in the XRD pattern of MCM-41/Fe_3O_4, which can be indexed to the (220), (311), (400), (422), (511), and (440) planes of the inverse spinel structure of Fe_3O_4.[51] Functionalization with MPTES and the subsequent thiol–ene click reaction with acrylic acid did not significantly alter the XRD pattern of MCM-41/Fe_3O_4–COOH, indicating that the crystalline nature of MCM-41/Fe_3O_4 was preserved throughout the functionalization steps. In addition, the crystallite size of Fe_3O_4 nanoparticles in the catalyst was estimated to be approximately 26 nm which was calculated using the Debye–Scherrer equation based on the XRD peak broadening. This value confirmed the nanoscale nature of Fe_3O_4 particles incorporated in the MCM-41 framework.

Nitrogen adsorption–desorption isotherm analysis was performed to investigate the textural properties and porosity changes of the synthesized materials. The isotherms of MCM-41, MCM-41/Fe_3O_4, and MCM-41/Fe_3O_4–COOH (Fig. 4) exhibited a typical type IV curve with a distinct hysteresis loop, confirming the presence of uniform mesoporous channels.[29] These results also affirmed that the stepwise functionalization preserved the overall mesostructure of the MCM-41 framework. Moreover, BET theory was conducted to evaluate the textural properties, including the specific surface area and the pore volume of the synthesized materials. The pristine MCM-41 exhibited a high specific surface area (1200 m^2 g^{-1}) and a large pore volume (0.9 mL g^{-1}), characteristic of its well-ordered mesoporous structure. A noticeable decrease in the surface area (900 m^2 g^{-1}) and the pore volume (0.7 mL g^{-1}) was observed for MCM-41/Fe_3O_4 compared to the bare MCM-41, which was attributed to partial pore blockage or occupation by Fe_3O_4 nanoparticles. The surface area (289 m^2 g^{-1}) and the pore volume (0.3 mL g^{-1}) of MCM-41/Fe_3O_4–COOH further reduced, consistent with the introduction of additional organic moieties within the mesoporous channels. Overall, these results corroborated the successful stepwise modification of MCM-41 while retaining its mesoporous nature.

TEM analysis was utilized to investigate the morphology and structural integrity of MCM-41, MCM-41/Fe_3O_4, and

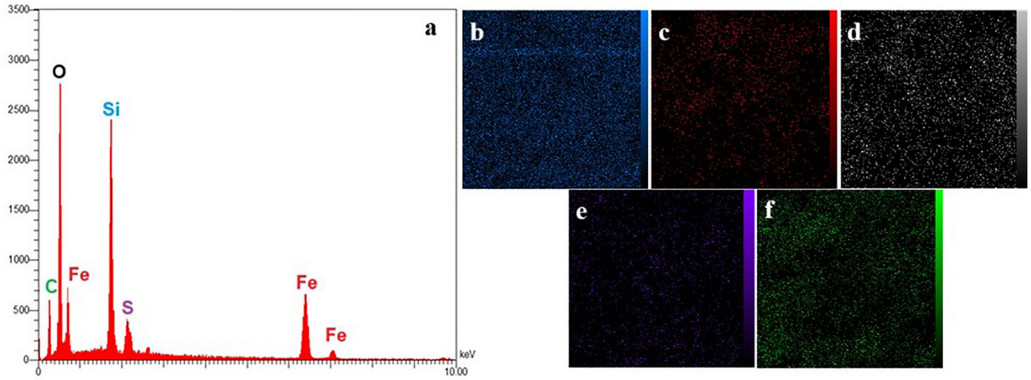

Fig. 2 EDX spectrum of MCM-41/Fe_3O_4–COOH (a) and the corresponding mapping images of Si (b), Fe (c), O (d), S (e), and C (f).

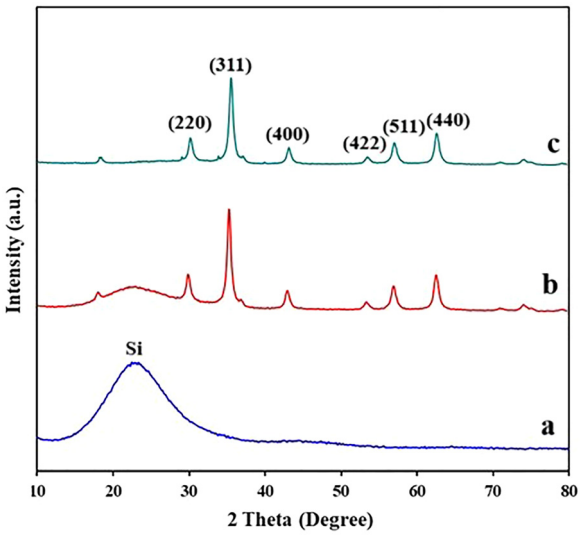

Fig. 3 XRD patterns of (a) MCM-41, (b) MCM-41/Fe_3O_4, and (c) MCM-41/Fe_3O_4–COOH.

MCM-41/Fe_3O_4–COOH (Fig. 5). The TEM image of pure MCM-41 revealed a uniform, well-ordered mesoporous structure with a hexagonal arrangement of pores, characteristic of the MCM-41 framework. In the TEM image of MCM-41/Fe_3O_4, dark contrast spherical particles were observed embedded within or attached to the silica matrix, confirming the successful integration of Fe_3O_4 nanoparticles without significant disruption of the mesoporous structure. In the case of MCM-41/Fe_3O_4–COOH, the overall morphology remained unchanged, although a slight increase in contrast and particle aggregation was noted, likely due to the presence of organic moieties on the surface. These observations confirmed the successful functionalization while maintaining the structural integrity and mesoporosity of the MCM-41/Fe_3O_4 nanocomposite. Besides, the SEM image of the MCM-41/Fe_3O_4–COOH (Fig. S1) showed a uniform spherical morphology, demonstrating the successful formation of the nanocomposite with a well-defined particle shape.

VSM analysis was employed to estimate the magnetic properties of MCM-41/Fe_3O_4 and MCM-41/Fe_3O_4–COOH (Fig. 6). Both samples exhibited clear superparamagnetic behavior with no remanence or coercivity. A decrease in the saturation magnetization value of MCM-41/Fe_3O_4–COOH compared to MCM-41/Fe_3O_4 was ascribed to the increased mass of non-magnetic organic layers in the catalyst. Despite the gradual decrease in magnetization, the catalyst retained sufficient magnetic responsiveness, enabling easy separation from the reaction mixture using a magnet.

TGA was performed to estimate the thermal stability and the presence of organic functional groups on the surface of the

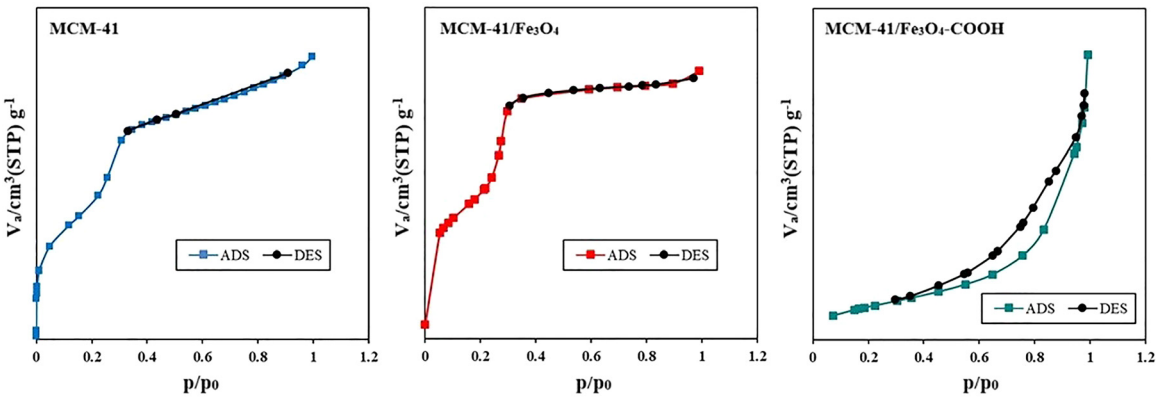

Fig. 4 N_2 adsorption–desorption isotherms of MCM-41, MCM-41/Fe_3O_4, and MCM-41/Fe_3O_4–COOH.

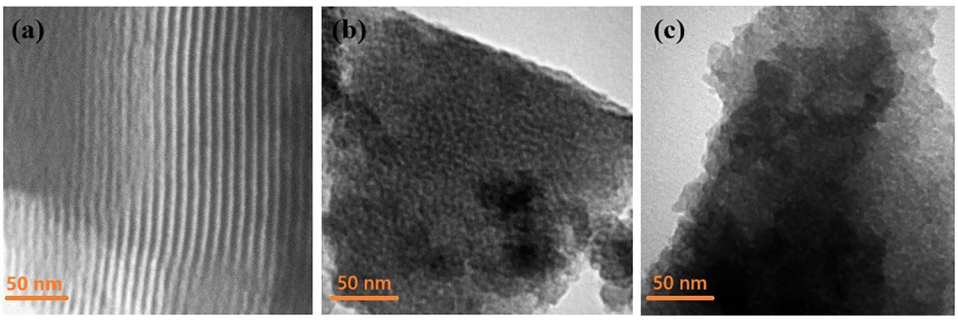

Fig. 5 TEM images of MCM-41 (a), MCM-41/Fe_3O_4 (b), and MCM-41/Fe_3O_4–COOH (c).

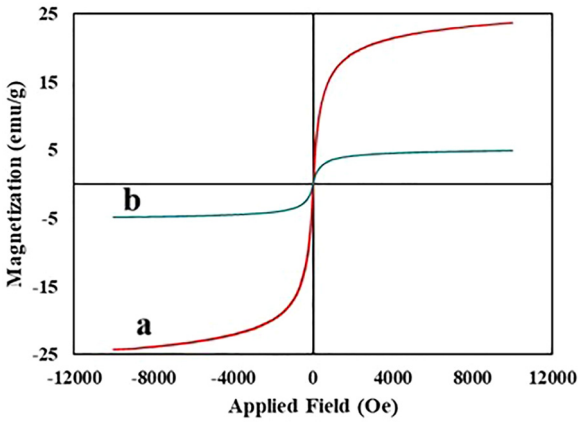

Fig. 6 VSM curves of MCM-41/Fe_3O_4 (a) and MCM-41/Fe_3O_4–COOH (b).

MCM-41/Fe_3O_4–COOH (Fig. 7). The TGA curve showed an initial weight loss of approximately 2% below 200 °C, which was ascribed to the removal of physically adsorbed water and residual solvents trapped within the mesoporous structure. A second significant weight loss was observed in the range of 200–700 °C, which was related to the thermal decomposition of the organic moieties introduced during surface functionalization, including the mercaptopropyl and carboxylic acid groups. Overall, the catalyst displayed good thermal stability up to 200 °C, beyond which the degradation of the grafted organic functionalities begins. This thermal behavior confirmed the successful functionalization of the catalyst and showed its suitability for catalytic applications under moderate thermal conditions.

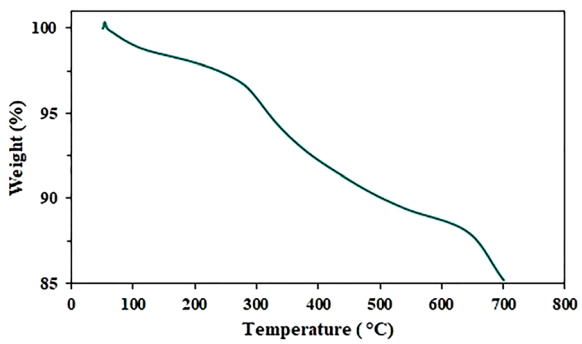

Fig. 7 TGA curve of MCM-41/Fe_3O_4–COOH.

The catalytic activity of MCM-41/Fe_3O_4–COOH was assessed in the conversion of fructose to 5-HMF. A systematic investigation of the solvent type, reaction temperature, reaction time, and catalyst loading was conducted to optimize the reaction conditions.

The choice of solvent plays a key role in the conversion of fructose to 5-HMF, influencing both 5-HMF yield and selectivity. To examine the impact of solvent on 5-HMF yield, the reaction was conducted in various solvents including dimethyl sulfoxide (DMSO), dimethylformamide (DMF), ethanol (EtOH), and water under identical conditions (120 °C, 40 min, 30 mg of catalyst). As can be seen in Fig. 8, the nature of solvent significantly influenced the 5-HMF yield. Among the examined solvents, DMSO provided the best 5-HMF yield (76%) due to its known capacity to suppress side reactions like rehydration of 5-HMF to levulinic acid or humin formation.[52] Moderate yield was obtained in DMF (61%), which could be ascribed to its lower ability to stabilize 5-HMF in comparison to DMSO. In contrast, ethanol and pure water resulted in significantly lower 5-HMF yields of 29% and 19%, respectively, likely due to faster 5-HMF degradation and construction of byproducts in these solvents.[53]

Although pure DMSO achieved the best 5-HMF yield, it is known that the use of DMSO/water mixtures can fine-tune the reaction environment, potentially enhancing 5-HMF yield. Previous studies have demonstrated that incorporating a controlled amount of water into DMSO can help moderate the dehydration kinetics of fructose and suppress unwanted side reactions by maintaining a favorable balance between dehydration and rehydration processes.[54] Motivated by these findings, we explored how water content affected 5-HMF yield in various DMSO/water mixtures. The reaction was carried out using DMSO/water mixtures with different volume ratios. Interestingly, the highest yield of 5-HMF (85%) was observed at a DMSO/water ratio of 2/1, which was slightly higher than the 5-HMF yield obtained in pure DMSO. However, when the water content was further increased (DMSO/water ratios of 1/1 and 1/2), a noticeable decline in 5-HMF yield was observed. This behavior was likely due to the enhanced rehydration of 5-HMF in the presence of excess water, leading to the formation of byproducts and humins.

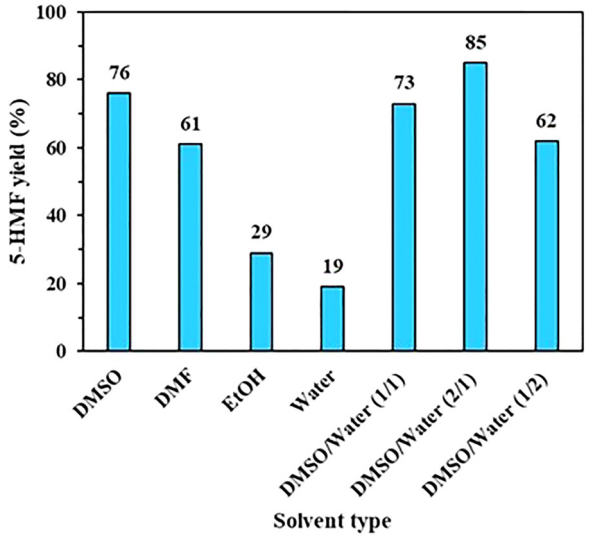

Fig. 8 Effect of the solvent type on the dehydration of fructose to 5-HMF. Reaction conditions: 100 mg of fructose, 30 mg of MCM-41/Fe_3O_4–COOH, 3 mL of solvent, 120 °C, 40 min.

The temperature-dependent behavior of the catalytic system was explored by carrying out the reaction at diverse temperatures (80, 100, 120, 140, and 160 °C). The results are summarized in Fig. 9a. At lower temperatures (≤100 °C), fructose dehydration proceeded slowly, resulting in lower 5-HMF yields. The maximum 5-HMF yield of 85% was attained at 120 °C, highlighting this as the optimal reaction temperature for effective fructose conversion to 5-HMF. However, further enhancing the temperature to 140 and 160 °C led to a slight decline in 5-HMF yield owing to the thermal degradation of 5-HMF and creation of humins or byproducts at elevated temperatures.[14]

To fix the optimal reaction time, the reaction was performed for varying durations of 10, 20, 40, 60 and 80 min at the optimized temperature of 120 °C using 30 mg of the catalyst. As presented in Fig. 9b, 5-HMF yield increased with time, reaching a maximum at 60 min (94%). Further extension of the reaction time to 80 min led to a slight reduction in 5-HMF yield (87%), which could be ascribed to the onset of side reactions like 5-HMF rehydration or humin formation under prolonged heating. These results confirmed that 60 min was the optimal reaction time for achieving the highest 5-HMF yield with minimal byproduct formation.

The impact of catalyst loading on the 5-HMF yield was examined by changing the catalyst quantity from 10 to 50 mg. The results revealed a significant influence of the catalyst amount on 5-HMF yield (Fig. 9c). In the presence of lower catalyst dosages (10 and 20 mg), 5-HMF yield was limited due to insufficient availability of active sites. As the catalyst quantity increased to 30 mg, a marked enhancement in 5-HMF yield was detected, which was attributed to the increased density of acid functionalities that facilitated the dehydration process. However, beyond 30 mg, the 5-HMF yield slightly decreased,

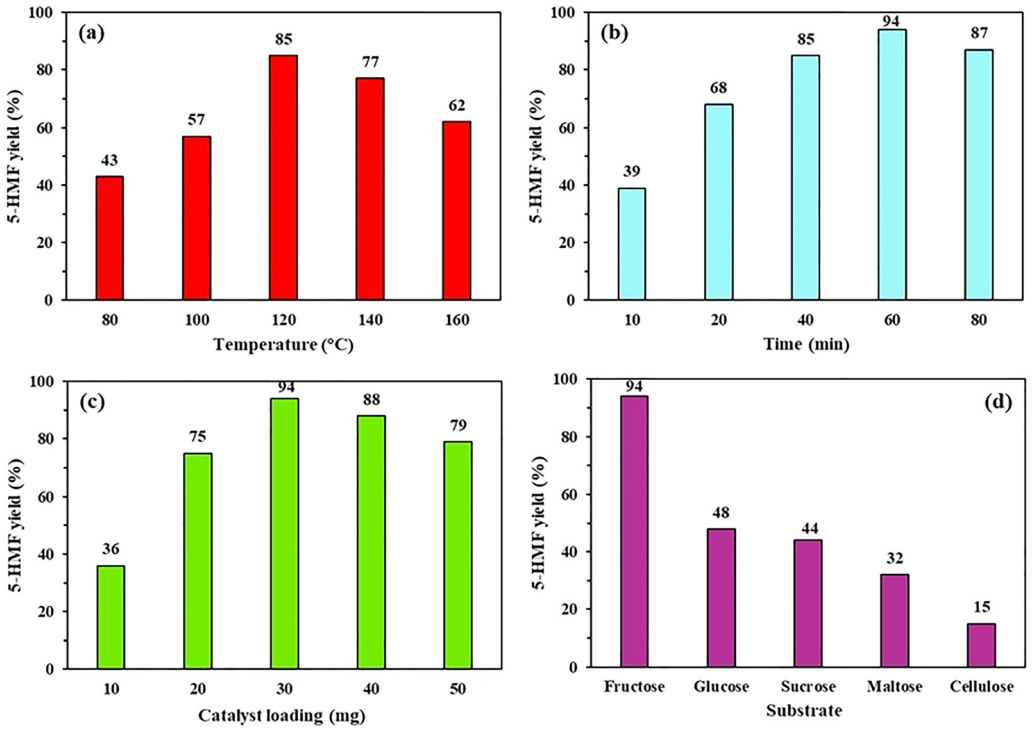

Fig. 9 Effects of (a) reaction temperature, (b) the reaction time, (c) catalyst loading, and (d) the substrate type on 5-HMF yield. Reaction conditions: (a) 100 mg of fructose, 30 mg of MCM-41/Fe_3O_4–COOH, 3 mL of DMSO/water (2/1, v/v), 40 min; (b) 100 mg of fructose, 30 mg of MCM-41/Fe_3O_4–COOH, 3 mL of DMSO/water (2/1, v/v), 120 °C; (c) 100 mg of fructose, 3 mL of DMSO/water (2/1, v/v), 120 °C, 60 min; and (d) 100 mg of substrate, 30 mg of MCM-41/Fe_3O_4–COOH, 3 mL of DMSO/water (2/1, v/v), 120 °C; 60 min.

possibly due to mass transfer limitations or side reactions promoted by excess acidic sites. Therefore, 30 mg of catalyst provided sufficient active sites for effective dehydration of fructose to 5-HMF. On the other hand, control experiments using MCM-41/Fe_3O_4 and MCM-41/Fe_3O_4-SH under the same reaction conditions revealed no detectable formation of 5-HMF, demonstrating that the presence of Fe_3O_4 nanoparticles and thiol groups alone was insufficient for catalyzing the dehydration of fructose and highlighting the essential role of the surface carboxylic acid groups in promoting the reaction.

The catalytic activity of MCM-41/Fe_3O_4–COOH was also investigated for the transformation of other carbohydrates like glucose, sucrose, maltose, and cellulose to 5-HMF under the optimal reaction conditions for the transformation of fructose into 5-HMF. The obtained results are provided in Fig. 9d. The catalyst exhibited the highest efficiency with fructose, achieving the maximum 5-HMF yield owing to the furanose structure of fructose, which undergoes direct dehydration under mild acidic conditions. In contrast, glucose yielded lower 5-HMF yield, which was attributed to the necessity of a prior isomerization step to fructose. Disaccharides like sucrose and maltose provided moderate 5-HMF yields, as their hydrolysis to monosaccharides is a prerequisite for effective dehydration. Among the tested substrates, cellulose gave the lowest 5-HMF yield, largely due to its crystalline structure and limited solubility, hindering effective catalytic interactions. These results demonstrated the effectiveness of the developed catalyst in the conversion of sugars to 5-HMF, particularly for monosaccharide substrates.

The recyclability of MCM-41/Fe_3O_4–COOH was examined through successive catalytic runs for the dehydration of fructose to 5-HMF under the optimal reaction conditions. After each run, the catalyst was magnetically separated, rinsed thoroughly with ethyl acetate and deionized water to remove any residual reactant or product, dried at 80 °C, and then reused without any further modification. As shown in Fig. 10, 5-HMF yield showed a slight decrease over five consecutive cycles. To further assess the stability of the acidic functional groups responsible for the catalytic activity, acid–base titration was performed to quantify the surface acidity of the used catalyst. The recovered catalyst after five runs demonstrated a slightly reduced acidity (0.64 mmol g^{-1}) compared to the fresh catalyst (0.69 mmol g^{-1}). Besides, the XRD pattern (Fig. S5) and the FT-IR spectrum (Fig. S6) of the recovered catalyst after five runs were almost the same as those of the fresh catalyst. The combined results from the recyclability test and acid–base titration suggested that MCM-41/Fe_3O_4–COOH was a stable catalyst for the dehydration of fructose to 5-HMF.

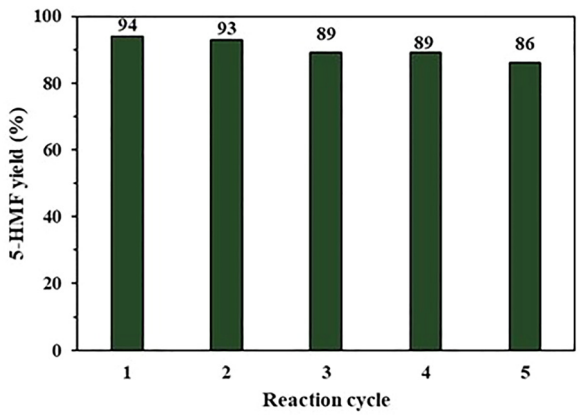

Fig. 10 Recyclability of MCM-41/Fe_3O_4–COOH in the conversion of fructose to 5-HMF. Reaction conditions: 100 mg of fructose, 30 mg of MCM-41/Fe_3O_4–COOH, 3 mL of DMSO/water (2/1, v/v), 120 °C, 60 min.

Table 1 Comparison of the catalytic activity of MCM-41/Fe_3O_4–COOH with that of several reported heterogeneous catalysts in the conversion of fructose to 5-HMF

Catalyst	Solvent	Temperature (°C)	Time (h)	5-HMF yield (%)	Ref.
SO_4^{2-}/TiO_2	DMSO	150	6	74.7	55
Al-KCC-1	DMSO	162	1	92.9	56
g-C_3N_4–SO_3H	DMSO	120	3	60	57
SiO_2-Imi-SO_3H-2	DMSO	120	8	74.1	58
Aquivion@silica	DMSO	120	1.5	85	59
MCM-41/Fe_3O_4–COOH	DMSO/water	120	1	94	This work

To validate the heterogeneous nature of MCM-41/Fe_3O_4-COOH, a hot-filtration test was performed. The reaction was conducted under optimized conditions (120 °C, 60 min) and after 30 min, the catalyst was rapidly removed from the reaction mixture *via* magnetic separation while maintaining the reaction temperature. The resulting catalyst-free filtrate was then allowed to continue reacting for the remaining 30 min under the same conditions. No significant increase in 5-HMF yield was observed after catalyst removal, demonstrating that the active catalytic species were not leached into the solution and confirming the heterogeneous nature of the catalyst.

As shown in Table 1, the catalytic activity of MCM-41/Fe_3O_4–COOH was found to be comparable or superior to that of several reported heterogeneous catalysts used for the dehydration of fructose to 5-HMF. Moreover, according to the experimental findings and supported by previous literature,[50] a probable reaction mechanism for the transformation of fructose into 5-HMF over MCM-41/Fe_3O_4–COOH is illustrated in Scheme 2.

4. Conclusions

Herein, a magnetically recoverable solid acid catalyst, MCM-41/Fe_3O_4–COOH, was successfully synthesized through surface modification of mesoporous silica MCM-41 with Fe_3O_4 nanoparticles and subsequently carboxylic acid groups *via* the thiol–ene click reaction. Comprehensive characterization techniques, including FT-IR spectroscopy, acid–base titration, EDX, XRD, BET, TEM, and VSM, established the successful incorporation of the magnetic nanoparticles, preservation of the mesoporous structure, and the presence of surface acid groups. The catalyst showed outstanding activity in the dehydration of fructose to 5-HMF, achieving a high yield of 94% at 120 °C using 30 mg of

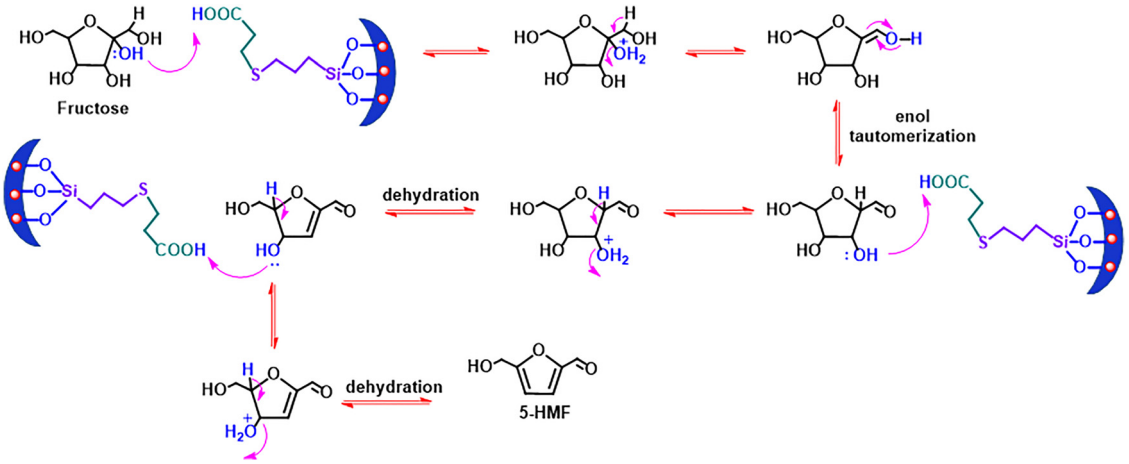

Scheme 2 Reaction mechanism for the dehydration of fructose to 5-HMF over MCM-41/Fe_3O_4–COOH.

catalyst for 60 min in a DMSO/H_2O (2 : 1 v/v) solvent system. The catalyst also demonstrated excellent stability and reusability, maintaining high efficiency over five consecutive cycles with only a slight decrease in 5-HMF yield. Overall, this study presents a promising, sustainable, and magnetically recoverable catalyst that combines the advantages of mesoporous materials with surface acidity and easy magnetic separation, showing great promise for application in biomass valorization.

Author contributions

A. R. M.: investigation, methodology, resources, conceptualization, and writing – original draft; S. B.: conceptualization, investigation, methodology, and writing – original draft; S. A.-H.: methodology, investigation, data curation, and writing – original draft; S. K. S.: data curation, investigation, and writing – original draft; S. R.: supervision, data curation, and writing – original draft; N. C. T.: visualization, data curation, and writing – original draft; A. S.: visualization and writing – original draft; V. J.: methodology, review and editing.

Conflicts of interest

The authors declare no competing financial interests.

Data availability

The data that support the findings of this study are available from the corresponding author upon reasonable request.

Supplementary information is available. See DOI: **https://doi.org/10.1039/d5nj02955d**.

References

1 J. Fan, X. Zhang, N. He, F. Song and X. Wang, *J. Environ. Chem. Eng.*, 2025, 117870.
2 X. Wang, H. Su and X. Liu, *Sustainability*, 2025, **17**, 6313.
3 K. Yang, C. Li, Q. Zhu, H. Wang and J. Qi, *Nanomaterials*, 2025, **15**, 524.
4 B. Li, X. Wang, A. Khurshid and S. F. Saleem, *Int. J. Environ. Sci. Technol.*, 2025, 1–14.
5 H. Hafizi, G. Walker and M. N. Collins, *Renewable Energy*, 2022, **183**, 459–471.
6 Q. Ye, Y. Chen, Y. Li, R. Jin, Q. Geng and S. Chen, *Dalton Trans.*, 2023, **52**, 12169–12184.
7 Y. Ma, B. Wang, H. Wang, X. Zhao, Y. Zhao, S. Wu and C. Xie, *Int. J. Hydrogen Energy*, 2025, **126**, 484–495.
8 Z. Yang, Y. Wen, P. Jiang, X. Peng, F. Zeng, H. Lin, L. Mu, X. Lu, T. Ji and J. Zhu, *ACS Sustainable Chem. Eng.*, 2025, **13**, 3374–3383.
9 K. Ravi, A. S. Singh, D. B. Pawara and A. V. Biradar, *Energy Fuels*, 2024, **38**, 18729–18736.
10 M. Kumar, R. Bains, A. S. Chauhan, A. Kumar and P. Das, *Renewable Energy*, 2025, **244**, 122657.
11 Y. Che, P. Lu, J. Zhang, X. Wang, Y. Liu, H. Yu and Y. Liu, *Fuel*, 2025, **388**, 134465.
12 P. Kang and R. K. Sharma, *Energy Fuels*, 2024, **38**, 23857–23863.
13 Z. Bi, X. Cui, H. Xu, Q. Li, D. Xu and Y. Guo, *Chem. Eng. J.*, 2025, 161613.
14 H. Guo, X. Ma, Z. Chen, J. Guo and J. Lu, *RSC Adv.*, 2025, **15**, 3664–3671.
15 M. Ansari, H. Jamali, R. Ghanbari, M. H. Ehrampoush, P. Zamani and B. Hatami, *Chem. Eng. J. Adv.*, 2025, 100718.
16 C.-Y. Hsu, A. Kumar, P. Kanjariya, A. Rajiv, A. Kashyap, H. M. Albert, S. Pokhriyal and M. Dehghanipour, *J. Alloys Compd.*, 2025, 179736.
17 J. Hua, M. Ji, P. Jiao, Z. Yin, Q. Xia, L. Jiang, J. Zhang and H. Pan, *Catalysts*, 2025, **15**, 396.
18 L. Xu, X. Pan, L. Gao, R. Wei, J. Li, X. Wen, Y. Li and G. Xiao, *Catal. Lett.*, 2025, **155**, 58.
19 C. Araya-Lopez, J. Conejeros, C. Valdebenito, R. Cabezas, G. Merlet, J. F. Marco, G. Abarca, R. Salazar and J. Romero, *ChemCatChem*, 2022, **14**, e202200046.
20 S. Wang, M. Zhang, D. Guo, J. Feng and H. Pan, *Fuel*, 2024, **363**, 130991.

21 Y. Zhang, B. Li, W. Guan, Y. Wei, C. Yan, M. Meng, J. Pan and Y. Yan, *Cellulose*, 2020, **27**, 3037–3054.
22 H. Xu, X. Li, W. Hu, L. Lu, J. Chen, Y. Zhu, H. Zhou and C. Si, *Fuel Process. Technol.*, 2022, **234**, 107338.
23 S. Xiong, Y. Guan, C. Luo, L. Zhu and S. Wang, *Energy Fuels*, 2021, **35**, 14462–14483.
24 S. Arumugam, N. Senthilkumar, N. Thirumalaivasan, G. Dharman, S. Pandiaraj, M. Rahaman, M. Palaniappan, R. Muthusami, T. Manogaran and L. Mari, *J. Organomet. Chem.*, 2023, **998**, 122804.
25 Q. Lu, S. Wang, C. Ji, G. Chen, J. Dong and F. Gao, *J. Porous Mater.*, 2024, **31**, 897–912.
26 A. Vasu, M. Naresh, G. K. Sai, Y. D. Rohini, B. Murali, M. Ramulamma, A. Ramunaidu and N. Narender, *Green Chem.*, 2021, **23**, 9439–9446.
27 G. Chaudhary, B. Joshi and A. P. Singh, *Inorg. Chem. Commun.*, 2024, **164**, 112405.
28 S. Pasricha, P. Gahlot, K. Mittal, D. Rai, N. Avasthi, H. Kaur and S. Rai, *ChemistrySelect*, 2022, **7**, e202103674.
29 B. Tahmasbi and A. Ghorbani-Choghamarani, *New J. Chem.*, 2019, **43**, 14485–14501.
30 R. Pourhasan Kisomi, F. Shirini and M. Golshekan, *Appl. Organomet. Chem.*, 2021, **35**, e6212.
31 M. Kalhor, P. Nozare, E. Vessally and B. Mohammadi, *ChemistrySelect*, 2023, **8**, e202301283.
32 M. Kalhor and Z. Zarnegar, *RSC Adv.*, 2019, **9**, 19333–19346.
33 M. Kalhor, M. Bigdeli and H. Moghanian, *Res. Chem. Intermed.*, 2023, **49**, 5375–5394.
34 M. Kalhor, Z. Vahedi and H. Gharoubi, *RSC Adv.*, 2023, **13**, 9208–9221.
35 M. Abdollahi-Alibeik and Z. Ramazani, *J. Chem. Sci.*, 2022, **134**, 77.
36 L. Z. Fekri and S. Zeinali, *Appl. Organomet. Chem.*, 2020, **34**, e5629.
37 L. Z. Fekri, K. H. Pour and S. Zeinali, *J. Organomet. Chem.*, 2020, **915**, 121232.
38 L. Z. Fekri, M. Nikpassand and M. Torabi, *Results Chem.*, 2025, **15**, 102258.
39 L. Zare Fekri, M. Nikpassand and S. Zeinali, *Org. Prep. Proced. Int.*, 2024, **56**, 257–263.
40 X. Xing, X. Shi, M. Ruan, Q. Wei, J. Li, Y. Guan, H. Gao and S. Xu, *Fuel*, 2024, **358**, 130106.
41 C. Yin, W. Chen, J. Zhang, M. Zhang and J. Zhang, *Sep. Purif. Technol.*, 2019, **210**, 175–181.
42 A. B. Lowe, *Polym. Chem.*, 2010, **1**, 17–36.
43 F. Raji, A. Saraeian, M. Pakizeh and F. Attarzadeh, *RSC Adv.*, 2015, **5**, 37066–37077.
44 G. Feng, W. Xie, F. Jiang, C. Shao, J. Yu, Q. Wu, Q. Zhang, Q. Yang, W. Jin and J. Liu, *Ceram. Int.*, 2023, **49**, 38148–38156.
45 V. M. Macedo, E. L. Gomes, J. C. Moreno-Pirajan, L. Giraldo, L. P. Tovar, S. I. Alves, L. A. Ruotolo and R. Fernandez-Felisbino, *ACS Omega*, 2023, **8**, 48181–48190.
46 R. Matos, I. Kuźniarska-Biernacka, M. Rocha, J. H. Belo, J. P. Araújo, A. C. Estrada, J. L. Lopes, T. Shah, B. A. Korgel and C. Pereira, *Catal. Today*, 2023, **418**, 114132.
47 T. Shafaati, M. Nikpassand, M. Mokhtary and L. Z. Fekri, *Appl. Organomet. Chem.*, 2024, **38**, e7470.
48 W. Xu and J.-Y. Liang, *Trans. Nonferrous Met. Soc. China*, 2025, **35**, 563–578.
49 G. Feng, W. Xie, E. Zheng, F. Jiang, Q. Yang, W. Jin, Q. Wu, J. Liu, D. Wang and Y. Huang, *Ceram. Int.*, 2024, **50**, 19757–19768.
50 R. Deplazes, C. Teles, C. Ciotonea, A. Sfeir, N. Canilho, F. Richard and S. Royer, *Catal. Today*, 2024, **430**, 114514.
51 S. K. Saraswat, A. M. Naglah, J. Makasana, H. A. Bakar, S. Ballal, M. K. Abosaoda, V. Kavitha, L. Bareja, P. N. Bhakuni and O. P. Doshi, *Sci. Rep.*, 2025, **15**, 12875.
52 J. Hao, X. Song, S. Jia, W. Mao, Y. Yan and J. Zhou, *Front. Energy Res.*, 2021, **9**, 679709.
53 S. Pumrod, N. Akkarawatkhoosith, T. Tongtummachat, A. Kaewchada, R. Chongcharoen and A. Jaree, *ACS Omega*, 2025, **10**, 15191–15203.
54 C. Jin, N. Xiang, X. Zhu, K. Sheng and X. Zhang, *Appl. Catal., B*, 2021, **285**, 119799.
55 R. Tomer and P. Biswas, *New J. Chem.*, 2020, **44**, 20734–20750.
56 F. Shahangi, A. N. Chermahini and M. Saraji, *J. Energy Chem.*, 2018, **27**, 769–780.
57 D. D. Le, T. H. Nguyen, D. A. Le Nguyen, H. B. Phan and P. H. Tran, *Energy Fuels*, 2024, **38**, 4203–4216.
58 V. T. C. Doan, T. M. Dao, T. A. Huynh and P. H. Tran, *RSC Adv.*, 2024, **14**, 17480–17490.
59 Y. Dou, S. Zhou, C. Oldani, W. Fang and Q. Cao, *Fuel*, 2018, **214**, 45–54.

